American Mineralogist, Volume 77, pages 62–75, 1992

Crystal field spectra and geochemistry of transition metal ions in silicate melts and glasses

HANS KEPPLER*
California Institute of Technology, Division of Geological and Planetary Sciences 170-25, Pasadena, California 91125, U.S.A.

ABSTRACT

The crystal field spectra of V^{3+}, Cr^{2+}, Cr^{3+}, Mn^{2+}, Mn^{3+}, Fe^{2+}, Co^{2+}, Ni^{2+}, and Cu^{2+} doped in glasses of albite and 50 wt% albite–50 wt% diopside composition were measured. The glasses were prepared at 1 atm pressure and under controlled f_{O_2} by quenching the corresponding silicate melts from 1200–1500 °C to room temperature. V^{3+} and Cr^{3+} occupy octahedral sites in the glasses. The sites of Cr^{2+}, Fe^{2+}, Ni^{2+}, and Cu^{2+} appear to be strongly distorted from ideal octahedral geometry. Co^{2+} is in distorted tetrahedral coordination. The fact that only Co^{2+} occupies a tetrahedral site can be understood on the basis of the small ionic radius and low octahedral site preference energy of Co^{2+}. A change of the melt composition from albite to 50 wt% albite–50 wt% diopside causes only a small increase in the crystal field splitting of the divalent ions, whereas Racah parameters and coordination numbers remain unchanged. However, the speciation of Cr in the glasses strongly depends on bulk composition. Spectroscopic evidence suggests the stabilization of Cr^{2+} in albite melt at 1500 °C even under very oxidizing conditions in equilibrium with air. In a series of Co^{2+}-doped glasses ranging in composition from pure albite to pure diopside, the strongest changes in the spectra of Co^{2+} occur between the composition of pure albite and 90 wt% albite–10 wt% diopside, while only minor changes are observed in the diopside-rich portion of the system. This observation is consistent with complexing of Co^{2+} by nonbridging O atoms in the melt. Published data of crystal-melt partition coefficients of Cr^{3+} and Ni^{2+} show that their partitioning behavior is essentially determined by the difference between the crystal field stabilization energy in the melt and in the crystal. Earlier theories that assumed the partitioning behavior of transition metal ions to be controlled by octahedral site preference energies disagree with spectroscopic evidence. In general, the more polymerized the melt, the more are transition metal ions expected to partition preferentially into crystalline phases.

INTRODUCTION

Although there are numerous experimental studies of the partitioning behavior of transition metal ions in magmatic processes (e.g., Barnes, 1986; Irving, 1978; Kinzler et al., 1990; Schreiber and Haskin, 1976; Takahashi, 1978), little information is available concerning the coordination and the chemical bonding of these ions in magmatic melts. Crystal field spectroscopy has been used with great success to investigate transition metal ions in minerals, and identical methods have been used in the study of glasses (e.g., Ahmed et al., 1983; Durán and Fernández Navarro, 1985; Fox et al., 1982; Goldman and Berg, 1980; Kojima et al., 1988; Lin and Angell, 1984; Nelson and White, 1980; Nelson and White, 1986; Nelson et al., 1983; Oyamada et al., 1987; Rao and Rao, 1986; Seth and Yadav, 1987; Turner and Turner, 1972; White and Knight, 1986; Wong and Angell, 1976). However, very few attempts have been made to apply these methods to quenched silicate melts of geologic relevance (Burns and Fyfe, 1964; Boon and Fyfe, 1972; Calas and Petiau, 1983). Therefore, this paper presents a systematic study of the crystal field spectra of glasses of the join albite-diopside doped with first-series transition metal ions.

The structure of these glasses corresponds to the structure of the liquid at the glass transformation temperature. This temperature ranges from approximately 800 to 1100 °C for the melt compositions and quench rates studied (Dingwell and Webb, 1990). It cannot be entirely ruled out that speciation changes occur at temperatures above the glass transformation temperature. In the present study, melts containing Co^{2+} and Ni^{2+} were quenched to room temperature with different quench rates, either by dropping the crucible with the melt into H_2O or by cooling it down slowly within about 5 min. The optical spectra of the samples subjected to such different quench rates were identical. The significance of this observation is, however, rather small. The different quench rates applied shift the glass transformation by less than 100 °C (Dingwell and Webb, 1990). Therefore, the experiments only show

* Present address: Bayerisches Geoinstitut, Universität Bayreuth, W-8580 Bayreuth, Germany.

0003–004X/92/0102–0062$02.00

that no major speciation change occurs over this rather small temperature range. Even the fastest accessible quench rates do not allow the sampling of silicate melt structures over the entire magmatic temperature range (Dingwell and Webb, 1990). Data on the behavior of melts above the glass transformation can only be obtained by direct measurements. Goldman and Berg (1980) studied the crystal field spectra of Fe^{2+} in a borosilicate glass at room temperature and in the corresponding melt at 1260 °C. No significant difference was observed. This is consistent with X-ray absorption studies of Fe in silicate melts and glasses (Waychunas et al., 1988). These measurements show little difference between the coordination of Fe^{2+} above and below the glass transformation temperature. Lin and Angell (1984), on the other hand, report temperature-dependent speciation changes of Ni^{2+} in potassium borate melts. In silicate melts of natural composition, however, Ni speciation in the melt appears to be essentially independent of temperature because the inherent temperature dependence of solid-melt partition coefficients of Ni is small (Hart and Davis, 1978; Kinzler et al., 1990). For the other transition metal ions, the available data are not sufficient to address the problem of speciation changes above the glass transformation. However, the data for Fe and Ni suggest that glasses are probably a good model for the behavior of these ions in melts.

Experimental methods

Starting materials

Starting materials were glass powders of albite or diopside composition and high-purity transition metal oxides (V_2O_5, Cr_2O_3, MnO_2, FeO, Co_3O_4, NiO, CuO). These components were mixed and ground in an agate mortar under ethanol.

Preparation of glass samples

The composition of most of the glasses studied was either albite or 50 wt% albite–50 wt% diopside (abbreviated albite-diopside). These compositions were chosen because the completely polymerized albite melt may serve as a simple model for granitic composition, whereas the albite-diopside melt has a degree of polymerization comparable to that of basalts. Batches of 250 mg to 1 g of the starting mixture were melted in a Pt crucible using a 1 atm high-temperature gas mixing furnace (Deltech). Temperature was measured by means of a Pt-PtRh thermocouple (type S) close to the crucible and f_{O_2} by means of an O_2 sensitive electrode. Experiments were performed in air, in pure O_2, or in H_2-CO_2 mixtures. After usually 12–24 h at 1200–1500 °C, samples were quenched by dropping the crucible into cold H_2O. Long experiment durations were chosen in order to obtain bubble-free or almost bubble-free glass slugs, which allow quantitative spectroscopic measurements of extinction coefficients. Durations were much longer than those commonly applied in studies of redox equilibria in similar systems (e.g., Mysen and Virgo, 1989). During the experiments, gas bubbles entrapped in the melt disappeared entirely or almost entirely; therefore, the reaction times were obviously sufficient to allow dissolved gases to diffuse out of and into the melt and to establish redox equilibrium with the surrounding gas reservoir. Moreover, the aim of the present study is not to measure redox equilibria but to determine the structural environment of a given ion in the glass. The rate of structural equilibration in silicate melts is given by the relaxation time. This time is below 10^{-6} s for the systems and temperatures investigated (Dingwell and Webb, 1990). Therefore, lack of equilibration is not a problem in this study.

It has been suggested (Dyar and Birnie, 1984; Dyar et al., 1987) that Fe^{3+}/Fe^{2+} ratios in glasses might depend on quench rates. One explanation for this observation could be redox reactions occurring at the glass surface in contact with the surrounding gas atmosphere. Such effects were not important in the present study because the surface layers of the glass slugs were not used for spectroscopic measurements. Another complication can arise if one element is present in different oxidation states. In this case, the rapid transfer of electrons from one site to another during quenching can alter the distribution of the ions over the available sites. However, in the present study, glasses were usually synthesized under conditions where only one oxidation state of the transition metal investigated is stable. Because of the absence of any electron donors or acceptors in the system, it is assumed that the oxidation state of the transition metal ions in the glasses was not affected by quenching.

Spectroscopic measurements and chemical analysis

Flat glass discs polished on both sides were prepared from glass chips of appropriate size. Spectroscopic measurements of these samples in the wavelength range from 300 to 2500 nm were carried out with a Cary 17 UV/VIS/NIR spectrometer. The chemical composition of the glasses was measured by electron microprobe (JEOL superprobe, 15 kV accelerating voltage, 30-nA specimen current, 30-s counting time, defocused beam). The following standards were used: albite (Na), forsterite (Mg), anorthite (Al, Si, Ca), garnet (Mn), fayalite (Fe), pure oxides (Cr, Ni), pure metals (V, Co, Cu). Chemical analyses were carried out on the same spots used for the spectroscopic measurements. Over the spot sizes required for recording the spectra (1–3 mm diameter), all samples were found to be homogeneous in composition.

Experimental results and discussion

The conditions of synthesis of the investigated glass samples are compiled in Table 1, and their chemical analyses are given in Table 2. Only one transition metal was doped into the glass at a time. Very small amounts of other transition metals as measured by electron microprobe might be artifacts of counting statistics and background correction. Measured Na contents in albite glasses tend to be somewhat below the stoichiometric value, and

Table 1. Synthesis relations for glass samples

Sample no.	Nominal composition of glass matrix	Doped ion	Temperature (°C)	Atmosphere	f_{O_2} (atm)	Duration (h)	Thickness of sample (mm)	Comments	Color of glass
S 2	Ab_{100}	Co^{2+}	1400	air	0.2	20	0.208	*	dark blue
S 3	Ab_{100}	Ni^{2+}	1400	air	0.2	22	0.489	*	brown
S 14	Ab_{100}	Mn^{2+}	1400	H_2-CO_2	$10^{-4.7}$	19	1.018		red brown
S 17	Ab_{100}	Cr^{2+}	1500	air	0.2	19	0.675	*	pale blue
S 18	Ab_{100}	Cu^{2+}	1200	O_2	1	20	0.416	*, **	green
S 33	$Ab_{50}Di_{50}$	Co^{2+}	1400	air	0.2	16	0.335		dark blue
S 34	$Ab_{50}Di_{50}$	Ni^{2+}	1400	air	0.2	21	0.761		brown
S 36	$Ab_{50}Di_{50}$	Cu^{2+}	1350	O_2	1	20	1.103	**	blue green
S 37	$Ab_{50}Di_{50}$	Cr^{2+}	1400	H_2-CO_2	$10^{-9.6}$	24	1.460		pale blue
S 39	$Ab_{50}Di_{50}$	V^{3+}	1500	H_2-CO_2	$10^{-8.8}$	21	2.794		brown
S 41	$Ab_{50}Di_{50}$	Cr^{3+}	1490	air	0.2	21	0.949	*	green
S 42	$Ab_{50}Di_{50}$	Mn^{3+}	1400	O_2	1	17	1.275	†	pale red
S 44	$Ab_{50}Di_{50}$	Mn^{2+}	1400	H_2-CO_2	$10^{-4.0}$	20	0.814		yellow
S 47	$Ab_{50}Di_{50}$	Fe^{2+}	1400	H_2-CO_2	$10^{-7.9}$	20	1.024		blue green
S 48	Ab_{100}	Fe^{2+}	1400	H_2-CO_2	$10^{-8.0}$	22	1.017		green brown
S 51	$Ab_{80}Di_{20}$	Co^{2+}	1400	air	0.2	16	0.244		dark blue
S 58	Di_{100}	Co^{2+}	1450	air	0.2	28	1.029		dark blue
S 59	$Ab_{90}Di_{10}$	Co^{2+}	1400	air	0.2	17	0.813	*	dark blue

Note: Compositions in wt%. Ab = albite, Di = diopside.
* Contains bubbles.
** Probably not all Cu as Cu^{2+}.
† Probably not all Mn as Mn^{3+}.

the same also holds for other glass compositions. This is apparently caused by a loss of Na by evaporation at high temperature. This effect was particularly strong if the sample was melted in a reducing atmosphere. In these cases, a loss of transition metals to the Pt crucible was also observed. Table 3 gives a compilation of observed optical absorption bands and their assignments. In cases where a sufficient number of bands were observed, Racah parameters and crystal field splittings were calculated using formulas given by König (1971). Energies of spin-forbidden transitions were obtained from Tanabe-Sugano diagrams given by Figgis (1966). The accuracy of band positions and crystal field splittings quoted is usually ± 100 cm^{-1} or better. Racah parameters, B, are believed to be accurate to ± 25 cm^{-1}.

Spectra of divalent ions

Cr^{2+}, d^4. The spectra of Cr^{2+} will be discussed later in connection with those of Cr^{3+}.

Mn^{2+}, d^5. The spectra of Mn^{2+} in glasses of albite and albite-diopside composition consist of only a weak band around 415 nm (Table 3, Fig. 1). The band is probably caused by the two transitions $^6A_{1g}(S) \rightarrow {}^4E_g(G)$ and $^6A_{1g}(S) \rightarrow {}^4A_{1g}(G)$ that are indistinguishable in energy. These transitions can occur in both tetrahedral and octahedral environments and are therefore not diagnostic for the coordination number. However, Mn^{2+}-containing silicate glasses subjected to UV radiation show a fluorescence that has been used for structural interpretations. According to Wong and Angell (1976), the fluorescence is caused

Table 2. Chemical analyses of glass samples (in wt%)

Sample no.	Na_2O	MgO	Al_2O_3	SiO_2	CaO	V_2O_3	Cr_2O_3	MnO	FeO	NiO	CoO	CuO	Total
S 2	8.35	—	19.25	69.04	0.03	—	—	—	0.03	—	1.00	—	97.7
S 3	7.92	—	19.42	70.80	0.03	—	—	—	0.03	0.93	—	0.03	99.2
S 14	8.21	0.01	18.83	67.16	0.03	—	0.05	4.89	0.03	—	—	0.02	99.2
S 17	9.13	—	19.51	69.86	0.03	—	0.18	0.07	0.03	0.02	—	0.05	98.9
S 18	8.77	—	19.06	67.73	0.04	—	—	—	0.03	—	—	0.81	96.4
S 33	5.71	7.92	9.74	62.52	13.23	—	—	0.01	0.12	—	0.96	0.06	100.3
S 34	5.62	7.80	9.57	62.04	13.13	—	—	0.02	0.02	0.86	—	0.01	99.1
S 36	5.85	7.88	9.56	61.87	13.17	—	—	—	0.01	0.01	0.01	0.45	98.8
S 37	4.50	7.90	9.85	63.36	13.46	0.02	0.16	0.02	0.03	—	—	—	99.3
S 39	2.59	7.97	10.03	65.12	13.70	0.10	0.03	—	0.01	—	—	—	99.5
S 41	5.68	8.06	9.69	63.07	13.43	0.02	0.09	—	0.05	0.03	0.01	0.03	100.2
S 42	5.86	8.07	9.61	62.68	13.42	—	—	0.38	0.02	—	—	0.04	100.1
S 44	5.90	7.71	9.32	60.19	12.74	0.01	0.02	4.76	0.23	0.01	—	0.02	100.9
S 47	5.33	7.68	9.58	62.81	12.81	0.02	—	—	2.49	—	—	—	100.7
S 48	6.99	0.04	19.26	69.49	0.04	—	—	0.02	3.97	—	—	0.02	99.8
S 51	8.38	3.17	15.36	66.74	5.21	—	0.02	0.01	0.13	—	0.94	—	100.0
S 58	0.09	15.66	0.04	56.48	26.41	0.01	—	—	0.08	—	0.90	0.02	99.7
S 59	8.60	1.64	17.33	68.16	2.63	0.02	—	0.03	0.09	—	0.88	0.01	99.4

Note: Measured contents below 0.01 wt% are indicated by dash.

TABLE 3. Spectroscopic data of transition metal ions in silicate glasses

Sample no.	Glass matrix	Band position (nm)	Band position (cm^{-1})	Extinction coeff. (ε) L/(mol·cm)	Band assignment
			Cr^{2+}-doped glasses		
S 17	Ab_{100}	625	16000	32	$^5E_g(D) \rightarrow {}^5T_{2g}(D)$
		490	20400	shoulder	
S 37	$Ab_{50}Di_{50}$	630	15900	27	$^5E_g(D) \rightarrow {}^5T_{2g}(D)$
		480	20800	shoulder	
			Mn^{2+}-doped glasses		
S 14	Ab_{100}	417	24000	0.39*	$^6A_{1g}(S) \rightarrow {}^4E_g(G)$ $^6A_{1g}(S) \rightarrow {}^4A_{1g}(G)$
S 44	$Ab_{50}Di_{50}$	415	24100	0.24*	$^6A_{1g}(S) \rightarrow {}^4E_g(G)$ $^6A_{1g}(S) \rightarrow {}^4A_{1g}(G)$
			Fe^{2+}-doped glasses		
S 48	Ab_{100}	1900	5260	very weak shoulder	$^5T_{2g}(D) \rightarrow {}^5E_g(D)$
		1100	9090	8.3	
S 47	$Ab_{50}Di_{50}$	1850	5400	shoulder	$^5T_{2g}(D) \rightarrow {}^5E_g(D)$
		1080	9260	13	
			Co^{2+}-doped glasses		
S 2	Ab_{100}	1680	5920 } barycenter		
		1520	6580 } 6660	19	$^4A_2(F) \rightarrow {}^4T_1(F)$
		1340	7460 }		
		664	15060	79	$^4A_2(F) \rightarrow {}^2T_1(G)$ $^4A_2(F) \rightarrow {}^2E(G)$
		600	16670	shoulder	$^4A_2(F) \rightarrow {}^4T_1(P)$
		495	20200	39	$^4A_2(F) \rightarrow {}^2T_2(G)$
S 33	$Ab_{50}Di_{50}$	1700	5880 } barycenter		
		1470	6800 } 7000	22	$^4A_2(F) \rightarrow {}^4T_1(F)$
		1200	8300 }		
		645	15500	shoulder	$^4A_2(F) \rightarrow {}^2T_1(G)$ $^4A_2(F) \rightarrow {}^2E(G)$
		591	16920	87	$^4A_2(F) \rightarrow {}^4T_1(P)$
		518	19300	58	$^4A_2(F) \rightarrow {}^2T_2(G)$
			Ni^{2+}-doped glasses		
S 3	Ab_{100}	1730	5780	9.6	$^3A_{2g}(F) \rightarrow {}^3T_{2g}(F)$
		1090	9170	8.2	$^3A_{2g}(F) \rightarrow {}^3T_{1g}(F)$
		640	15620	19	$^3A_{2g}(F) \rightarrow {}^1E_g(D)$
		535	18690	shoulder	$^3A_{2g}(F) \rightarrow {}^3T_{1g}(P)$
		460	21740	44	
S 34	$Ab_{50}Di_{50}$	1900	5260	4.4	$^3A_{2g}(F) \rightarrow {}^3T_{2g}(F)$
		980	10200	4.1	$^3A_{2g}(F) \rightarrow {}^3T_{1g}(F)$
		630	15870	shoulder	$^3A_{2g}(F) \rightarrow {}^1E_g(D)$
		540	18520	shoulder	$^3A_{2g}(F) \rightarrow {}^3T_{1g}(P)$
		446	22420	41	
			Cu^{2+}-doped glasses		
S 18	Ab_{100}	790	12660	n.m.	$^2E_g(D) \rightarrow {}^2T_{2g}(D)$
S 36	$Ab_{50}Di_{50}$	780	12820	n.m.	$^2E_g(D) \rightarrow {}^2T_{2g}(D)$
			V^{3+}-doped glasses		
S 39	$Ab_{50}Di_{50}$	635	15700	shoulder	$^3T_{1g}(F) \rightarrow {}^3T_{2g}(F)$
		460	21700	18	$^3T_{1g}(F) \rightarrow {}^3T_{1g}(P)$
			Cr^{3+}-doped glasses		
S 41	$Ab_{50}Di_{50}$	650	15400	18	$^4A_{2g}(F) \rightarrow {}^4T_{2g}(F)$
		435	23000	30	$^4A_{2g}(F) \rightarrow {}^4T_{1g}(F)$
			Mn^{3+}-doped glasses		
S 42	$Ab_{50}Di_{50}$	730	13700	n.m.	$^5E_g(D) \rightarrow {}^5T_{2g}(D)$
		467	21400	n.m.	

Note: Compositions in wt%. Ab = albite, Di = diopside. Band positions quoted are believed to be accurate to ±100 cm^{-1}. All ions are in octahedral (Cr^{3+}, V^{3+}) or distorted octahedral (Cr^{2+}, Fe^{2+}, Ni^{2+}, Mn^{3+}) coordination except Co^{2+}, which is in a distorted tetrahedral site. Coordination is not precisely known for Mn^{2+}. Extinction coefficients should be considered to be only approximate. Densities of glasses used for the calculation of extinction coefficients were estimated on the basis of data given in Bansal and Doremus (1986; albite glass = 2.4 g/cm^3; albite-diopside glass = 2.6 g/cm^3). No extinction coefficients are given for Cu^{2+} and Mn^{3+} because some Cu^+ and Mn^{2+}, respectively, might be present in the samples. The abbreviation n.m. = not measured.

* These data are not very reliable because of difficulties in making the background correction.

by a transition from the excited $^4T_{1g}(G)$ state to the $^6A_{1g}(S)$ ground state. The energy of this transition strongly depends on field strength and therefore coordination number. Both the Mn^{2+}-doped albite and albite-diopside glasses display a weak pink fluorescence. This is believed to be diagnostic (Wong and Angell, 1976) for octahedral Mn^{2+} whereas tetrahedral Mn^{2+} would cause an intensive green fluorescence. However, different interpretations of the emission spectra of Mn^{2+} in glasses have been suggested (Nelson and White, 1980). Therefore, the significance of data obtained from optical spectroscopy for Mn^{2+} is uncertain. Kohn et al. (1990) investigated the structural environment of Mn^{2+} in dry and hydrous silicate glasses using X-ray absorption spectroscopy. They found undistorted octahedral coordination of Mn^{2+} in a hydrous silica glass. In the other compositions studied, Mn^{2+} appears to

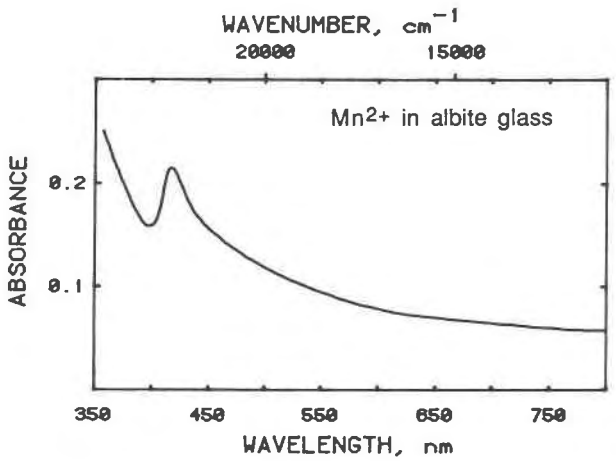

Fig. 1. Spectrum of Mn^{2+} in albite glass (sample S 14, thickness 1.018 mm, 3.79 wt% Mn).

be either in a very distorted site or distributed over different sites. Cooney and Sharma (1990) suggested, based on Raman spectra, that an unknown, possibly small proportion of Mn^{2+} occupies tetrahedral sites in orthosilicate glasses.

Fe^{2+}, d^6. Spectra of Fe^{2+} in albite and albite-diopside melt are shown in Figure 2 (compare Table 3). The spectra consist of a strong band close to 1100 nm and a weak shoulder around 1900 nm. The bands near 1100 nm can only be caused by octahedral Fe^{2+}, as this is the typical absorption range of the transition $^5T_{2g}(D) \rightarrow {}^5E_g(D)$ of octahedral Fe^{2+} in many silicates, such as olivines, pyroxenes, and amphiboles (e.g., Goldman and Rossman, 1977; Rossman, 1988). Two different possibilities exist for the origin of the band near 1900 nm: it could be caused by tetrahedral Fe^{2+} or it could be a component of the $^5T_{2g}(D) \rightarrow {}^5E_g(D)$ transition of octahedral Fe^{2+}, being split into two components by a distortion of octahedral geometry. If the band were caused by tetrahedral Fe^{2+}, the fraction of Fe^{2+} in tetrahedral sites would be very small because of the low band intensity and because the extinction coefficient for tetrahedral Fe is expected to be much higher than ϵ for octahedral coordination (Figgis, 1966). However, it is very likely that no significant amount of tetrahedral Fe^{2+} is present at all, and the band is indeed caused by Fe^{2+} in distorted octahedral coordination. Tetrahedral Fe^{2+} in spinels absorbs at 2000 nm (Mao and Bell, 1975). Spinels have densely packed structures with short cation-O distances. These distances will surely be significantly larger in a silicate glass. This should shift the band of tetrahedral Fe^{2+} to lower energies and wavelengths above 2000 nm. The observed band in the glass spectra is therefore unlikely to be caused by Fe^{2+} in tetrahedral coordination. Moreover, because of its degenerate ground state, Fe^{2+} is expected to show some distortion in an octahedral environment, which should cause a splitting of the $^5T_{2g}(D) \rightarrow {}^5E_g(D)$ transition into two components. In many crystalline silicates such as pyroxenes

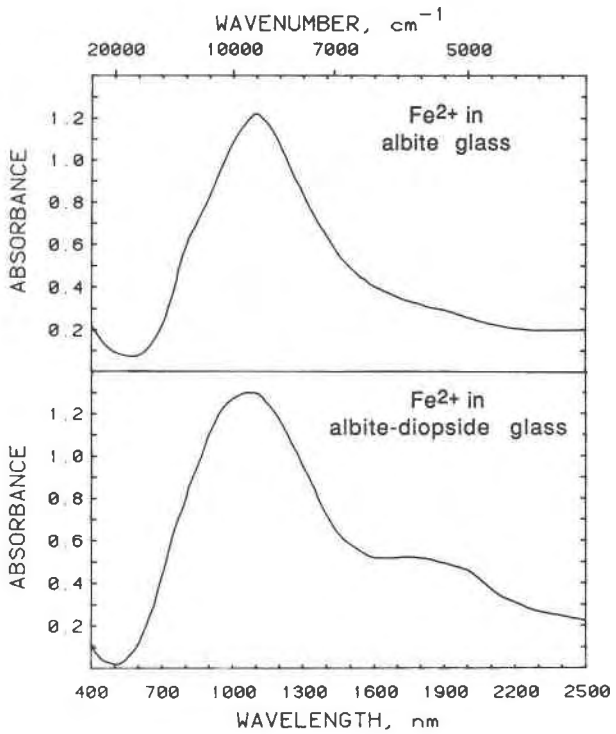

Fig. 2. **(above)** Spectrum of Fe^{2+} in albite glass (sample S 48, thickness 1.017 mm, 3.08 wt% Fe). **(below)** Spectrum of Fe^{2+} in albite-diopside glass (sample S 47, thickness 1.024 mm, 1.98 wt% Fe).

and amphiboles (Goldman and Rossman, 1977; Rossman, 1988), one component of this transition absorbs around 2000 nm. Therefore, it is most likely that both bands observed in the spectra of Fe^{2+}-doped glasses are caused by the transition $^5T_{2g}(D) \rightarrow {}^5E_g(D)$ of Fe^{2+} in a distorted octahedral site. This assignment yields a crystal field splitting Δ for Fe^{2+} of 7170 cm^{-1} in albite glass and of 7330 cm^{-1} in albite-diopside glass. The E_g term is split by 3830 cm^{-1} in albite and by 3860 cm^{-1} in albite-diopside glass by a distortion of the octahedral coordination. The splitting of the ground state is neglected in this treatment.

It has been suggested (Calas and Petiau, 1983) that the band at 1900 nm cannot be caused by a distorted octahedral environment because its half-width is much smaller than for the 1100 nm band. This appears to be misleading. The width of a band is determined by variations in field strength due to thermal vibrations that change the distance between the d orbitals of Fe^{2+} and surrounding O atoms. Because different O atoms in a strongly distorted site have different structural environments and form bonds of different strength, there is no reason why the amplitudes of their vibrations should be equal. In a distorted octahedral site, electronic transitions from the e_g orbitals to the d_{z^2} or $d_{x^2} - {}_{y^2}$ orbital will therefore be broadened to a different extent, depending on the vibrational amplitudes of the O atoms that are closest to the maximum charge density of these orbitals.

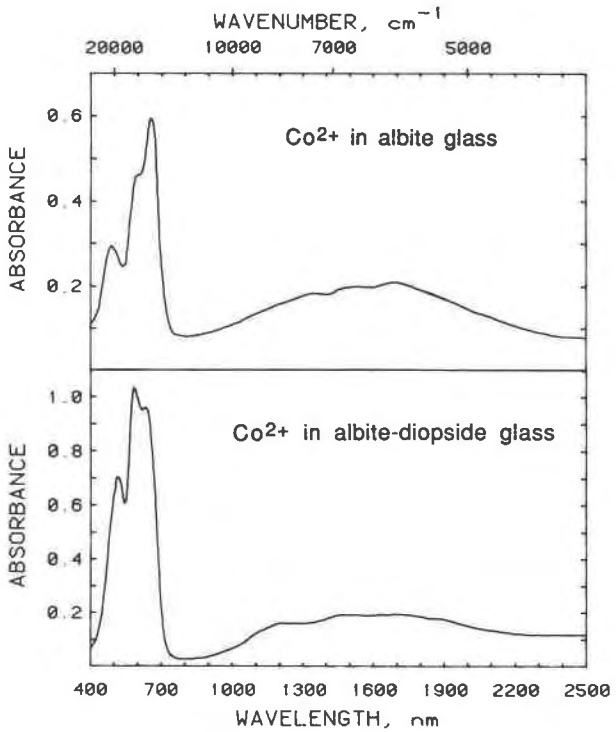

Fig. 3. **(above)** Spectrum of Co^{2+} in albite glass (sample S 2, thickness 0.208 mm, 0.79 wt% Co, contains bubbles). **(below)** Spectrum of Co^{2+} in albite-diopside glass (sample S 33, thickness 0.335 mm, 0.75 wt% Co).

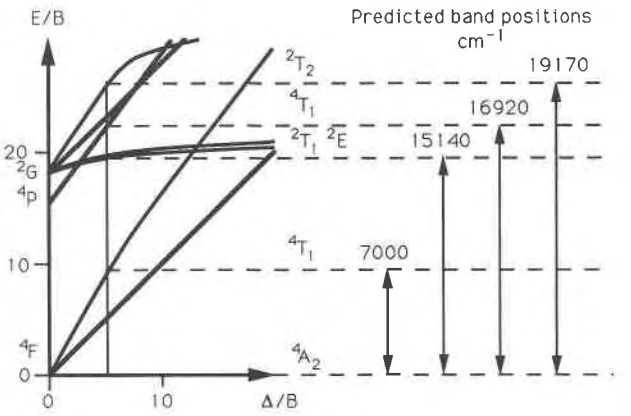

Fig. 4. Tanabe-Sugano diagram for tetrahedral Co^{2+} (after Figgis, 1966) with predicted band positions for B = 787 cm^{-1}, Δ = 4040 cm^{-1} (albite-diopside glass).

The intensity ratio of the two main band components observed in the spectra of Fe^{2+} in glasses changes only slightly over a very wide range of matrix compositions (Boon and Fyfe, 1972; Fox et al., 1982). This would be highly unlikely if these bands were caused by two different species. The low extinction coefficients of Fe^{2+} in the glasses studied (Table 3) also rule out a large deviation from centrosymmetry for the Fe^{2+} site.

Waychunas et al. (1988) investigated the coordination of Fe^{2+} in melts and glasses of $Na_2FeSi_3O_8$ and $K_2FeSi_3O_8$ composition and concluded that Fe^{2+} is a four-coordinated network-former in these glasses. Cooney and Sharma (1990) suggested a similiar structural role of Fe^{2+} in fayalite glass. As there might be a compositional effect on Fe^{2+} speciation, these data cannot be directly applied to the glasses studied in the present paper. However, the low coordination numbers and Fe-O bond distances found by Waychunas et al. could also be due to a distribution of Fe^{2+} over octahedral sites with variable distortion. Such a situation is realized in the crystal structure of fayalite. EXAFS analyses of fayalite yield Fe-O distances that are significantly too short and coordination numbers close to four rather than six (Waychunas et al., 1986).

Mössbauer spectroscopy was used in numerous studies to investigate the coordination of Fe^{2+} and Fe^{3+} in glasses (e.g., Dyar and Birnie, 1984; Dyar et al., 1987; Mysen and Virgo, 1989; Spiering and Seifert, 1985). However, the isomer shift ranges of tetrahedral and octahedral Fe^{2+} overlap considerably (Waychunas et al., 1988), and also the spectra are poorly resolved with respect to assigning individual site occupancies.

Co^{2+}, d^7. The spectra of glasses containing Co^{2+} (Fig. 3, Table 3) are dominated by a strong band system around 600 nm. Both the splitting of this band into three components and the high extinction coefficients are diagnostic for tetrahedral Co^{2+} (Wong and Angell, 1976; Figgis, 1966). Tetrahedral coordination of Co^{2+} in glasses showing this optical absorption system was confirmed by X-ray diffraction studies (Corrias et al., 1986). The component close to 600 nm in the center of this band system can be assigned to the spin-allowed transition $^4A_2(F) \rightarrow {}^4T_1(P)$ (compare Table 3). The bands near 650 and 500 nm are due to two spin-forbidden transitions (Wong and Angell, 1976). The best fit of measured band positions is obtained by assigning one to $^4A_2(F) \rightarrow {}^2T_1(G)$ and $^4A_2(F) \rightarrow {}^2E(G)$, which are very close in energy, and by assigning the other band to $^4A_2(F) \rightarrow {}^2T_2(G)$ (Table 3, Fig. 4). These spin-forbidden bands appear at relatively high intensity because the doublet states involved are very close in energy to $^4T_1(P)$. This apparently allows some mixing of these wave functions, greatly increasing the probability of transitions from the ground state to the doublet states. The separation of the three components of the band system in the visible range of the spectrum appears to be too high to be caused by the splitting of one band as a result of spin-orbit coupling, as proposed by Nelson and White (1986). The weak band in the infrared region of the Co^{2+}-doped glasses can be assigned to $^4A_2(F) \rightarrow {}^4T_1(F)$. This band is split into three submaxima, which is probably caused by a low symmetry distortion of the coordination tetrahedron, lifting the degeneracy of the $^4T_1(F)$ state. This interpretation is supported by the observation that the energy separation of the components depends on glass composition (Table 3), which would not be expected if the fine structure were caused by spin-orbit coupling, as suggested by Nelson and White (1986). A tetragonal

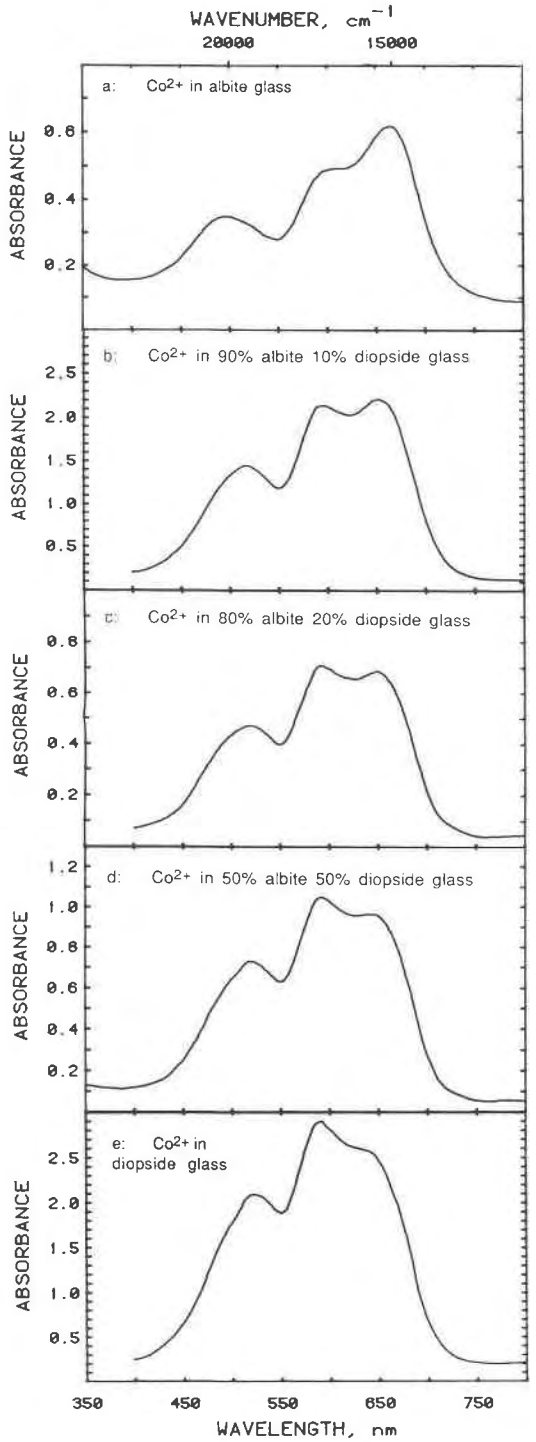

Fig. 5. Spectra of Co^{2+} in glasses ranging from pure albite to pure diopside composition. (**a**) Co^{2+} in albite glass (sample S 2, thickness 0.208 mm, 0.79 wt% Co, contains bubbles). (**b**) Co^{2+} in 90 wt% albite–10 wt% diopside glass (sample S 59, thickness 0.813 mm, 0.69 wt% Co, contains bubbles). (**c**) Co^{2+} in 80 wt% albite–20 wt% diopside glass (sample S 51, thickness 0.244 mm, 0.74 wt% Co). (**d**) Co^{2+} in 50 wt% albite–50 wt% diopside glass (sample S 33, thickness 0.335 mm, 0.75 wt% Co). (**e**) Co^{2+} in diopside glass (sample S 58, thickness 1.029 mm, 0.71 wt% Co).

Table 4. Crystal field spectra of Co^{2+} in glasses

	Albite glass (S 2) Δ = 3830 cm^{-1}, B = 789 cm^{-1}		Albite-diopside glass (S 33) Δ = 4040 cm^{-1}, B = 787 cm^{-1}	
Transition	Observed energy (cm^{-1})	Predicted energy (cm^{-1})	Observed energy (cm^{-1})	Predicted energy (cm^{-1})
$^4A_2(F) \rightarrow {}^4T_1(F)$	6660*	6660	7000*	7000
$^4A_2(F) \rightarrow {}^2T_1(G)$	15060	15130	15500	15140
$^4A_2(F) \rightarrow {}^2E(G)$				
$^4A_2(F) \rightarrow {}^4T_1(P)$	16670	16670	16920	16920
$^4A_2(F) \rightarrow {}^2T_2(G)$	20200	19040	19300	19170

Note: Distorted tetrahedral coordination is assumed. To account for the distortion, the barycenter of the band corresponding to $^4A_2(F) \rightarrow {}^4T_1(F)$ was used for fitting of Δ and B. Spin-forbidden bands were predicted on the basis of Racah parameters C/B = 4.5, which is slightly too high for Co^{2+} (Figgis, 1966). The error introduced by this approximation is probably small.
* Barycenter of split band.

or trigonal distortion would not entirely left the degeneracy of $^4T_1(F)$; therefore a low symmetry distortion seems to be present. On the basis of this interpretation, crystal field splittings, Δ and Racah parameters, B, can be calculated for Co^{2+} in albite and albite-diopside glass. To account for the distortion, the barycenter of the three components of the band in the infrared was used for the calculation. This yields Δ = 3830 cm^{-1} for albite and Δ = 4040 cm^{-1} for albite-diopside composition. The value of B for albite is 789 cm^{-1}, and for albite-diopside it is 787 cm^{-1}. The difference between the two values for B is smaller than experimental error and therefore insignificant. The value of B is reduced to 70% of the free ion value. Predicted and measured band positions for Co^{2+} in albite and albite-diopside glass are compared in Table 4.

Although there is only a small influence of glass composition on the magnitude of the crystal field splitting, very subtle changes in the environment of the Co^{2+} ion can be detected using crystal field spectra. The relative intensities of the three bands in the visible range strongly depend on the energy separation of the doublet states from the $^4T_1(P)$ state and therefore on the crystal field splitting. Figure 5 shows the visible region of the crystal field spectra of Co^{2+} in glasses ranging in composition from pure albite to pure diopside. The spectra change significantly as a function of glass composition. The component close to 650 nm that is strongest in albite glass loses intensity as the diopside content in the matrix increases and forms only a weak shoulder in the spectrum of diopside glass. On the other hand, the band near 600 nm, which is weak in albite glass, becomes the strongest band in the diopsidic matrix. The magnitude of these changes is not equally distributed over the composition range. The strongest changes occur in the very albite-rich portion of the system, between pure albite and 90% albite–10% diopside. Hardly any change is observed in the diopside-rich part of the system. Nelson and White (1986) investigated the crystal field spectra of Co^{2+} over a wide range of sodium silicate compositions. They found that

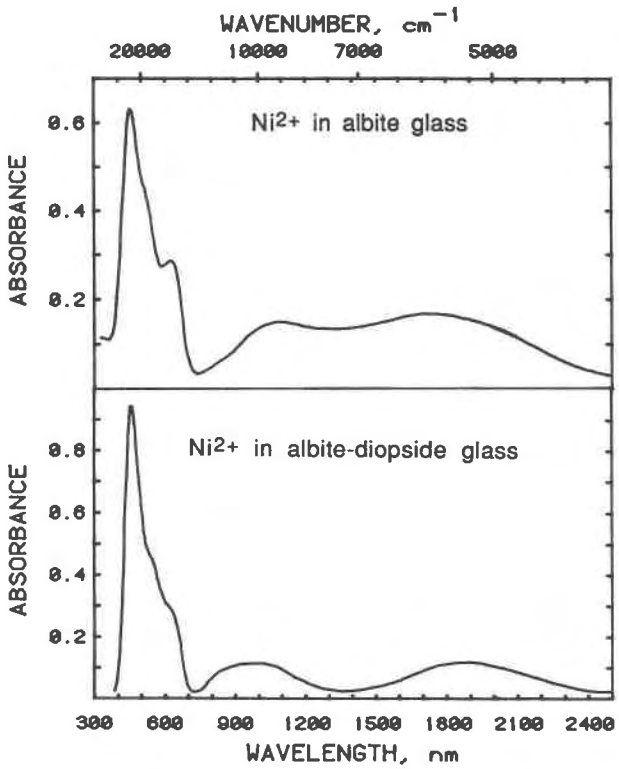

Fig. 6. (**above**) Spectrum of Ni^{2+} in albite glass (sample S 3, thickness 0.489 mm, 0.93 wt% Ni, contains bubbles). (**below**) Spectrum of Ni^{2+} in albite-diopside glass (sample S 34, thickness 0.761 mm, 0.86 wt% Ni).

the spectra are essentially independent of glass composition. As the glass structure changes considerably over the range of compositions studied, Nelson and White suggested that Co^{2+} forms a distinct tetrahedral complex in these glasses. This explains why the spectra of Co^{2+} are hardly affected by changes in the structure of the glass matrix. Similar structural models have been suggested for other transition metal ions (Nelson and White, 1980; Nelson et al., 1983; White and Knight, 1986). Complexing of Co^{2+} with nonbridging O atoms fully accounts for the changes in the spectra of Co^{2+} in glasses of the join albite-diopside reported in this study. In the diopside-rich portion of this system, the concentration of nonbridging O atoms is high; therefore Co^{2+} forms a tetrahedral complex in the glass. It is only when the matrix composition approaches albite composition that the concentration of the nonbridging O atoms becomes so small that Co^{2+} takes on a different structural environment.

It cannot be ruled out that the glasses studied contain a small amount of octahedrally coordinated Co^{2+}, the spectral features of which could be hidden below the much stronger bands of the tetrahedral species. However, the proportion of octahedral Co^{2+} cannot be large because in this case the measured extinction coefficients would be reduced below the values expected for a tetrahedrally coordinated ion. This is not observed.

TABLE 5. Crystal field spectra of Ni^{2+} in glasses

Transition	Albite glass (S 3) Δ = 5330 cm^{-1}, B = 893 cm^{-1}		Albite-diopside glass (S 34) Δ = 6000 cm^{-1}, B = 845 cm^{-1}	
	Observed energy (cm^{-1})	Predicted energy (cm^{-1})	Observed energy (cm^{-1})	Predicted energy (cm^{-1})
$^3A_{2g}(F) \rightarrow {}^3T_{2g}(F)$	5780	5330	5260	6000
$^3A_{2g}(F) \rightarrow {}^3T_{1g}(F)$	9170	9170	10200	10200
$^3A_{2g}(F) \rightarrow {}^1E_g(D)$	15620	15180	15870	14520
$^3A_{2g}(F) \rightarrow {}^3T_{1g}(P)$	20215*	20215	20470*	20470

Note: Tetragonally distorted octahedral coordination is assumed. To account for the distortion, the barycenter of the band corresponding to $^3A_{2g}(F) \rightarrow {}^3T_{1g}(P)$ is used for fitting of Δ and B. The transition $^3A_{2g}(F) \rightarrow {}^3T_{2g}(F)$ cannot be measured precisely and is not used for the calculation. The spin-forbidden band is predicted using Racah parameters $C/B = 4.71$.
* Barycenter of split band.

Ni^{2+}, d^8. The spectra of Ni^{2+}-doped glasses (Fig. 6, Table 3) consist of two bands in the infrared region and one strong band in the visible region. In addition, there are two weak components on the low-energy side of the latter band. The three stronger bands obviously correspond to the spin-allowed transitions $^3A_{2g}(F) \rightarrow {}^3T_{2g}(F)$, $^3A_{2g}(F) \rightarrow {}^3T_{1g}(F)$, and $^3A_{2g}(F) \rightarrow {}^3T_{1g}(P)$ of Ni^{2+} in an octahedral field. The weak component around 630–640 nm can be assigned to the spin-forbidden transition $^3A_{2g}(F) \rightarrow {}^1E_g(D)$. The most likely explanation for the shoulder near 540 nm is a distortion of the coordination octahedron that partially lifts the degeneracy of $^3T_{1g}(P)$ and therefore causes a splitting of $^3A_{2g}(F) \rightarrow {}^3T_{1g}(P)$ into two components. The band at 640 nm, which is assigned to a spin-forbidden transition, is not likely to be caused by the splitting of $^3T_{1g}(P)$ because this would require such a strong distortion that a splitting of the two bands in the infrared should result, but such a splitting is not observed. If $^3T_{1g}(P)$ is split into only two components, the distortion of the octahedron must be of relatively high symmetry, probably tetragonal. Observed band positions and those predicted on the basis of the given band assignment are compared in Table 5. This table also contains data for the crystal field splittings and Racah parameters. The Racah parameters, B, are close to 80% of the free ion value, indicating high ionicity of the chemical bond. Generally, the spectra of the Ni^{2+}-doped glasses (Fig. 6) are very similiar to the spectra of many complex oxides containing Ni^{2+} in distorted octahedral sites (Rossman et al., 1981). There is also a great similarity with the spectrum of Ni^{2+}-doped olivine (Hu et al., 1990). Because X-ray diffraction studies show that these substances all contain Ni^{2+} in octahedral or distorted octahedral sites, there is no basis for assigning some of the bands in Ni^{2+}-containing albite or albite-diopside glass to transitions of tetrahedral Ni^{2+}, as was proposed by Burns and Fyfe (1964).

Based mainly on X-ray absorption measurements, Galoisy and Calas (1991) recently suggested Ni^{2+} to be in fivefold coordination in silicate glasses. However, as pointed out above in the discussion of Fe^{2+}, X-ray absorption measurements are very sensitive to disorder ef-

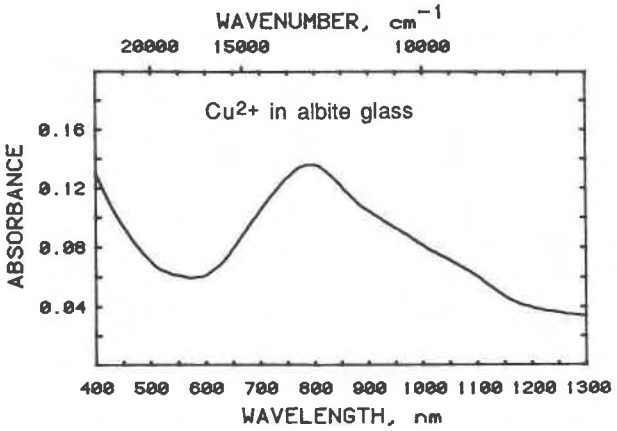

Fig. 7. Spectrum of Cu^{2+} in albite glass (sample S 18, thickness 0.416 mm, 0.65 wt% Cu, contains bubbles, probably not all Cu present as Cu^{2+}).

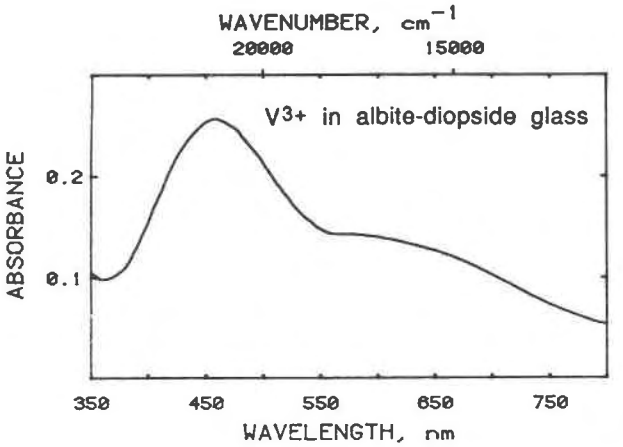

Fig. 8. Spectrum of V^{3+} in albite-diopside glass (sample S 39, thickness 2.794 mm, 0.07 wt% V).

fects, which can lead to calculated coordination numbers and cation-O distances being systematically too low. The optical spectra of Ni^{2+}-doped glasses do not support the assumption of fivefold coordination for Ni^{2+}. Energy level diagrams for Ni^{2+} in trigonal-dipyramidal coordination have been calculated by Ciampolini (1966). They predict a total of five spin-allowed transitions, three of which should be observed between 5000 and 15000 cm^{-1}. The spectra of trigonal-dipyramidal Ni^{2+} complexes agree well with this prediction (Furlani, 1968; Wood, 1972; Morassi et al., 1973). However, the spectrum of Ni^{2+} in albite-diopside glass (Fig. 6) clearly shows only two bands in this range, as expected for octahedral geometry. In addition, the extinction coefficients for Ni^{2+} in the glasses investigated are well within the range found for crystalline compounds containing octahedral Ni^{2+} (Rossman et al., 1981), although a five-coordinated site without a center of symmetry should cause much higher extinction coefficients (Figgis, 1966).

Cu^{2+}, d^9. The spectra of albite and albite-diopside glasses containing Cu^{2+} show one broad and asymmetric absorption band close to 800 nm (Fig. 7). This is the typical absorption range of octahedral Cu^{2+} in many glasses (Ahmed et al., 1983; Durán and Fernández Navarro, 1985; Seth and Yadav, 1987). Tetrahedral Cu^{2+} would be expected to absorb at lower energies around 1800 nm, assuming that the crystal field splitting in the tetrahedral field is about 4/9 of the octahedral value. The asymmetry of the band [$^2E_g(D) \rightarrow {}^2T_{2g}(D)$] is caused by distortion. The position of the band maximum yields a crystal field splitting of 12660 cm^{-1} for albite and 12820 cm^{-1} for albite-diopside glass. These data are, however, somewhat unreliable, as the magnitude of distortion is unknown and not considered in the determination of the crystal field splitting. A distorted octahedral environment of Cu^{2+} in glasses showing similiar absorption spectra was confirmed by EPR (Calas and Petiau, 1983).

Spectra of trivalent ions

V^{3+}, d^2. The spectrum of V^{3+} in albite-diopside glass (Fig. 8) is similiar to the spectra of many silicates and oxides containing V^{3+} in an octahedral site (Schmetzer, 1982). The strong band at 460 nm can be assigned to $^3T_{1g}(F) \rightarrow {}^3T_{1g}(P)$, the shoulder at 635 nm to $^3T_{1g}(F) \rightarrow {}^3T_{2g}(F)$ in an octahedral field. This yields a crystal field splitting of 16700 cm^{-1} and a Racah parameter, B, of 469 cm^{-1} (55% of free ion value).

Cr^{3+}, d^3 and Cr^{2+}, d^4. In magmatic systems, Cr can occur in two oxidation states, Cr^{3+} and Cr^{2+}. Cr^{3+} is the usually stable oxidation state, whereas Cr^{2+} is normally only found under very reducing conditions (Schreiber and Haskin, 1976; Schreiber et al. 1978). Figure 9a shows the spectra of Cr^{3+} in albite-diopside glass quenched from a melt at about 1500 °C equilibrated with air. Divalent Cr is stable in this matrix only under very reducing conditions (Fig. 9b). To stabilize more than 90% of dissolved Cr in the divalent state in basaltic melts, f_{O_2} values close to the iron-wüstite buffer are necessary at 1500 °C (Schreiber et al., 1978). The change of oxidation state from Cr^{3+} to Cr^{2+} causes a conspicuous change of the color of Cr-doped glasses from green to blue. Surprisingly, quenching a Cr-doped albite melt equilibrated with air at 1500 °C yields a blue glass, and the spectrum (Fig. 9c) is virtually identical with that of Cr^{2+} in albite-diopside matrix. To demonstrate the presence of Cr^{2+} in this glass, a series of experiments with Cr-doped albite melts was carried out at 1500 °C under different f_{O_2}, ranging form that of air ($f_{O_2} = 0.2$) to $f_{O_2} = 10^{-10}$. Quenching of the melts always yielded blue glasses, and the spectra remained essentially unchanged over the entire range of f_{O_2} studied. This result makes the presence of any oxidation state other than Cr^{2+} rather unlikely. To account for the blue color of some synthetic diopside crystals, Schreiber (1977) invoked the presence of Cr^{4+}. However, if Cr^{4+} were present in the blue albite glass studied, glasses pre-

pared under more reducing conditions should show the spectra of Cr^{3+} and Cr^{2+}, which was not observed. Moreover, the optical spectra of the few well-characterized compounds known to contain Cr^{4+} do not agree very well with the spectra of the glasses (Alyea et al., 1971).

Schreiber et al. (1978) observed a dependence of the Cr^{3+}-Cr^{2+} redox equilibrium on composition with more polymerized melts stabilizing Cr^{2+} relative to Cr^{3+}, which is consistent with the apparent stabilization of Cr^{2+} in albite melt in equilibrium with air reported in the present paper. According to White and Knight (1986), Cr^{3+} forms a distinct complex with nonbridging O atoms in silicate glasses. Therefore, the Cr^{2+}-Cr^{3+} redox equilibrium is expected to depend on the concentration of nonbridging O atoms. In albite melt, which ideally contains no nonbridging O atoms, this effect will shift the Cr^{3+}-Cr^{2+} equilibrium toward Cr^{2+}. The spectroscopic data presented in this paper suggest that the crystal field stabilization of transition metal ions is generally higher in albite-diopside than in albite melt. Because of the extraordinarily high crystal field stabilization energy (CFSE) of Cr^{3+}, the reduction of CFSE in albite melt as compared with that of albite-diopside composition will also tend to stabilize Cr^{2+} relative to Cr^{3+}.

The spectrum of Cr^{3+} in albite-diopside glass (Fig. 9a) shows the two bands expected for the octahedrally coordinated ion, which correspond to the transitions $^4A_{2g}(F) \rightarrow {}^4T_{2g}(F)$ and $^4A_{2g}(F) \rightarrow {}^4T_{1g}(F)$ (Table 3). The energies of these transitions yield a crystal field splitting of 15400 cm^{-1} and a Racah parameter $B = 837$ cm^{-1}. The crystal field splitting in the glass is almost identical with that in pyroxenes, and the Racah parameters are similiar (Burns, 1985).

The spectra of Cr^{2+} (Figs. 9b and 9c, Table 3) consist of one band and a weak shoulder. The shoulder seems to be a feature of Cr^{2+} and is apparently not caused by the presence of Cr^{3+}, which could cause a similiar absorption, because in a series of albite glasses prepared under different f_{O_2} (ranging from 0.2 to 10^{-10}), the spectrum remained essentially unchanged. The spectrum can be satisfactorily explained by the transition $^5E_g(D) \rightarrow {}^5T_{2g}(D)$ of Cr^{2+} in a distorted octahedral site. The distortion causes a splitting of $^5E_g(D)$, which explains the appearance of a shoulder in addition to the main band. This interpretation is supported by the similiarity of the glass spectra to those of Cr^{2+}-doped olivine and Cr_2SiO_4 (Scheetz and White, 1972). The magnitude of the crystal field splitting can be estimated from the barycenter of the absorption bands. This yields 18200 cm^{-1} for albite and 18350 cm^{-1} for albite-diopside composition. However, these data are only approximate, as the precise nature of the octahedral distortion and therefore the splitting of $^5E_g(D)$ are not known.

Mn^{3+}, d^4. Mn^{3+} was obtained in albite-diopside glasses equilibrated at 1400 °C with pure O_2 (Fig. 10). The spectrum is similiar to that of Mn^{3+} in the distorted octahedral site of andalusite (Rossman, 1988). The two bands result from the splitting of the transition $^5E_g(D) \rightarrow {}^5T_{2g}(D)$

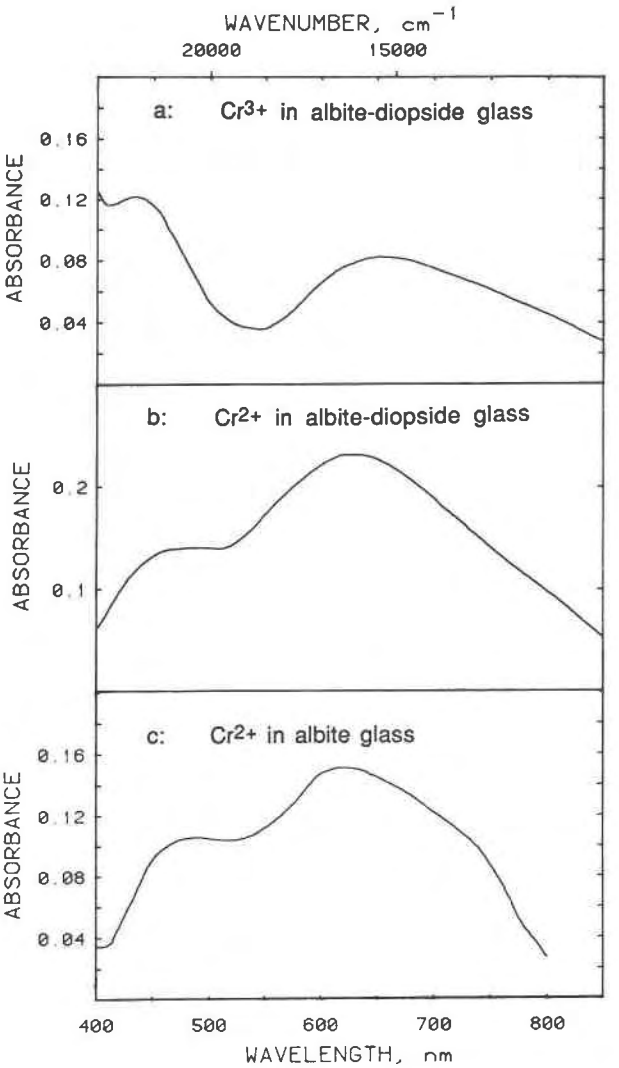

Fig. 9. (a) Spectrum of Cr^{3+} in albite-diopside glass (sample S 41, thickness 0.949 mm, 0.06 wt% Cr, contains bubbles). (b) Spectrum of Cr^{2+} in albite-diopside glass (sample S 37, thickness 1.460 mm, 0.11 wt% Cr). (c) Spectrum of Cr^{2+} in albite glass (sample S 17, thickness 0.675 mm, 0.13 wt% Cr, contains bubbles).

by distortion of the octahedral coordination, as it was discussed for the isoelectronic Cr^{2+}. The barycenter of the two bands yields a crystal field splitting of 17550 cm^{-1}. Heating of Mn-doped albite melts in O_2 always yielded glasses that contained tiny opaque crystals of octahedral shape. These crystals are probably a spinel rich in hausmannite (Mn_3O_4) component. As in the case of Cr, the trivalent oxidation state of Mn could not be obtained in albite glass.

Discussion

Co^{2+} is the only transition metal ion investigated that predominantly occupies tetrahedral sites in albite and albite-diopside glass, whereas all other ions appear to be in

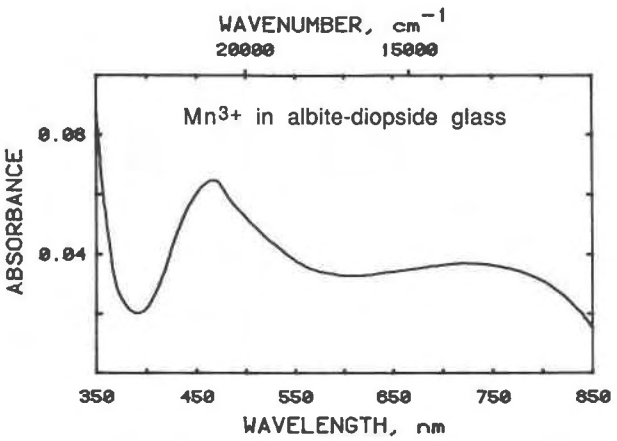

Fig. 10. Spectrum of Mn^{3+} in albite-diopside glass (sample S 42, thickness 1.275 mm, 0.29 wt% Mn, probably not all Mn present as Mn^{3+}).

octahedral or distorted octahedral coordination, although the presence of a small amount of these ions in tetrahedral sites cannot be entirely ruled out. The behavior of Co^{2+} can easily be understood on the basis of crystal field theory. Table 6 gives the ionic radius and octahedral site preference energy for the divalent ions of Co and its two neighbors in the periodic table, Fe and Ni. Of the three ions, Fe^{2+} has the largest ionic radius, apparently making it too big to fit into a tetrahedral site. Ni^{2+}, on the other hand, has the smallest ionic radius but an extraordinarily high octahedral site preference energy, which explains why Ni^{2+} occupies octahedral sites in the glass. Apparently, only in the case of Co^{2+} are both the ionic radius and the octahedral site preference energy low enough to allow tetrahedral coordination of this ion.

Network-forming cations (Si^{4+}, Al^{3+}) in silicate glasses are generally tetrahedrally coordinated. The fact that Co^{2+} also occupies tetrahedral sites does not imply that it is a network former. Rather, the fact that the spectrum of Co^{2+} does not change over a wide range of compositions of sodium silicate melts (Nelson and White, 1986) and the similiar observation reported in the present paper for diopside-rich compositions of the join albite-diopside suggest that Co^{2+} forms a distinct tetrahedral complex in the melt.

Ions having d^4 (Cr^{2+}, Mn^{3+}), d^6 (Fe^{2+}), and d^9 (Cu^{2+}) configuration have a degenerate ground state and are therefore expected to be subject to Jahn-Teller distortion. The spectra of all these ions indeed indicate a strongly distorted octahedral environment. It would be misleading, however, to assume that the distortion is exclusively caused by the Jahn-Teller effect. Rather, the distortion seems at least partially to result from steric constraints imposed by the structure of the glass matrix. This idea is supported by spectroscopic evidence outlined above that suggests distorted octahedral coordination of Ni^{2+} in both albite and albite-diopside glass. Octahedral Ni^{2+} has completely filled t_{2g} orbitals and half filled e_g orbitals. As a distortion does not change the barycenters of t_{2g} or e_g, no additional stabilization results from this effect. The spectra of V^{3+}, Cr^{3+}, and Mn^{2+} show no apparent signs of a distorted coordination for these ions. This does not rule out the possibility that some distortion is present, and resulting band splittings simply cannot be resolved.

The question arises whether ions like Ni^{2+}, which are not subject to the Jahn-Teller effect, only occupy distorted sites because more regular sites are already filled. If that were the case, one would expect to see a dependence of the spectra on the concentration of the doped transition metal ions. However, experiments with variable amounts (0.1–1 wt%) of Ni^{2+} and Co^{2+} doped in glasses did not show this effect.

If the spectra of divalent ions in albite and albite-diopside glass are compared (Table 7), it becomes obvious that there is only a small effect of glass composition on the crystal field parameters. The variations in the Racah parameter, *B*, are probably insignificant, indicating an essentially unchanged ionicity of the chemical bond. The crystal field splittings of the ions generally seem to be larger in albite-diopside than in albite glass, although the effect is small. This points to cation-O distances being slightly smaller in albite-diopside than for albite composition.

TABLE 6. Ionic radius and octahedral site preference energy (OSPE) for Fe^{2+}, Co^{2+}, and Ni^{2+}

	Ionic radius (Å)	OSPE (kJ/mol)
Fe^{2+}	0.78	11.6
Co^{2+}	0.74	29.0
Ni^{2+}	0.69	60.6

Note: Ionic radii for sixfold coordination according to Shannon (1976). OSPEs were calculated from the crystal field splittings of Fe^{2+}, Co^{2+}, and Ni^{2+} in albite-diopside glass, assuming that the crystal field splitting in tetrahedral coordination is approximately 4/9 of the value for octahedral coordination.

Geological applications

It has been suggested (Burns and Fyfe, 1964; Burns, 1970; Henderson and Dale, 1970) that the partitioning of transition metal ions between crystalline phases and silicate melts is essentially determined by the octahedral site preference energy (OSPE) of the ions. This is based on the assumption that transition metals generally occupy both tetrahedral and octahedral sites in magmas, whereas they are exclusively octahedrally coordinated in rock-forming minerals. Therefore, the transfer of an ion from the liquid into the solid state should be accompanied by a gain in energy that is determined by the octahedral site preference energy, that is, the difference between the crystal field stabilization energy in an octahedral and in a tetrahedral field. However, the spectroscopic data on transition metal ions in silicate glasses presented in this paper show that all ions, with the exception of Co^{2+}, are in an octahedral environment. There is no evidence that would suggest the presence of a substantial number of these ions in tetrahedral sites. Even if a small fraction of

TABLE 7. Crystal field splittings Δ ($\pm$100 cm^{-1}) and Racah parameters B ($\pm$25 cm^{-1}) for first series transition metal ions in albite and albite-diopside glass

	Albite glass			Albite-diopside glass		
	Coordination	Δ (cm^{-1})	B (cm^{-1})	Coordination	Δ (cm^{-1})	B (cm^{-1})
V^{3+}	—	—	—	O_h	16700	469
Cr^{3+}	—	—	—	O_h	15400	837
Mn^{3+}	—	—	—	dist. O_h	17550	—
Cr^{2+}	dist. O_h	18200	—	dist. O_h	18350	—
Mn^{2+}	O_h	—	—	O_h	—	—
Fe^{2+}	dist. O_h	7175	—	dist. O_h	7330	—
Co^{2+}	dist. T_d	3830	789	dist. T_d	4040	787
Ni^{2+}	dist. O_h	5330	893	dist. O_h	6000	845
Cu^{2+}	dist. O_h	12660*	—	dist. O_h	12820*	—

Note: dist. = distorted, O_h = octahedral, T_d = tetrahedral, dash = not measured.

* These data are not very reliable, as the distortion could not be considered in the calculation of Δ. The real magnitude of Δ is probably smaller than the number given.

a transition metal occupied tetrahedral sites, this would not be sufficient to change significantly the bulk thermodynamic properties of the dissolved ion, which determine the partitioning behavior. The octahedral site preference energy can therefore not account for the partitioning behavior of transition metal ions.

It is not obvious that partition coefficients can be understood using crystal field theory because the crystal field stabilization usually accounts only for approximately 10–30% of the total bonding energy of an ion (Figgis, 1966). Partition coefficients are determined by the difference of the bonding energy of an ion in the crystal and in the melt. The bonds in the two phases essentially differ by the cation-anion distance r; distortions can also be considered to be variations of r. The electrostatic Coulomb interaction potential between the ions varies with r^{-1}; however, the magnitude of the crystal field splitting, and therefore the crystal field stabilization energy, varies with r^{-5} (e.g., Burns, 1985). This shows that if two sites with different r are compared, the difference of bonding energy of an ion in these sites will be largely determined by the difference of the crystal field stabilization energies (CFSE), at least for ions having a high CFSE, such as Ni^{2+} and Cr^{3+}.

This hypothesis can easily be tested. Table 8 compares the Nernst distribution coefficients for Ni^{2+} and Cr^{3+} between basaltic melt and different minerals, as measured and as calculated from spectroscopic measurements of CFSE in glasses and crystals. In this calculation, it was simply assumed that $\ln K_d = -\Delta G/RT$ and $\Delta G = \Delta$(CFSE). Although this treatment is oversimplified because Nernst coefficients were used instead of real equilibrium constants, the calculated data reproduce the measured partition coefficients within a factor of about 3 or better and essentially correctly predict the relative magnitudes of the partition coefficients for different minerals. This suggests that the crystal-melt partitioning of Ni^{2+} and Cr^{3+} is largely determined by the difference between CFSE in melt and in crystals. In a qualitative way, this was already pointed out by Calas and Petiau (1983).

Calas and Petiau (1983) also found a decrease of crystal field splitting and CFSE of transition metal ions with increasing polymerization of the melt, which is in agreement with the results of the present study. They suggested that this compositional dependence of CFSE might be partially responsible for the change of crystal-melt partition coefficients with changing melt composition and for the partitioning of transition metals between coexisting immiscible melts. In general, the more polymerized the melts, the more are transition metal ions expected to partition preferentially into crystalline phases. If two immiscible melts are in equilibrium, the less polymerized melt will contain the higher concentrations of transition metals. Both effects are observed (Irving, 1978; Watson, 1976). However, most of the compositional dependence of partition coefficients disappears if true equilibrium constants

TABLE 8. Nernst distribution coefficients of Ni^{2+} and Cr^{3+} between crystalline phases and basaltic melt

	$CFSE_{crystal}$ (cm^{-1})	$CFSE_{crystal} - CFSE_{melt}$ (kJ/mol)	K_d calculated 1500 K	K_d measured
Ni^{2+}—CFSE in quenched albite-diopside melt: 7200 cm^{-1}				
Olivine (M1)	9500	27.5	9.1	5–15 for most basaltic compositions; Kinzler et al. (1990)
Enstatite, low calcium pyroxene (M1)	8280	12.9	2.8	1–10, mostly ca. 3; Irving (1978) 7.4; Colson et al. (1988)
Diopside	10800	43.1	32	2–11; Irving (1978)
Spinels	12840	67.5	225	5.1–51; Irving (1978)
Cr^{3+}—CFSE in quenched albite-diopside melt: 18480 cm^{-1}				
Olivine	20280	21.5	5.6	0.2–1.4; Schreiber and Haskin (1976)
Enstatite, low calcium pyroxene	18460	−0.2	1.0	2–14; Barnes (1986) 4–9; Schreiber and Haskin (1976)
Diopside	18600	1.4	1.1	3; Schreiber and Haskin (1976)
Spinels	22220	44.8	36	51–500; Irving (1978) ca. 100; Barnes (1986)

Note: $K_d = c_{crystal}/c_{melt}$, in weight ratios. Spectroscopic data for crystalline phases from Burns (1985). CFSE of Ni^{2+} in spinels was estimated using data for corundum. Measured partition coefficients are given for a range of melt compositions and temperatures. Older literature on partition coefficients is summarized in Irving (1978). Coefficients calculated using spectroscopic data for CFSE in glasses and minerals and as measured in experimental studies.

are used instead of Nernst coefficients (e.g., Colson et al., 1989). The spectroscopic data presented in this paper and by Calas and Petiau (1983) suggest that there must be an intrinsic dependence of the partitioning equilibria on melt composition, even when the partitioning is described by thermodynamically valid equilibrium constants.

Acknowledgments

This study was carried out during an 18-month visit in the laboratory of Peter J. Wyllie at Caltech, made possible by a grant from NATO obtained through the German Academic Exchange Service (DAAD). Funding for laboratory expenses was provided by NSF grant EAR-8904375, given to Peter J. Wyllie.

I am greatly indebted to Peter J. Wyllie for supporting my work and to George Rossman for many fruitful discussions and for permission to use his spectroscopic facilities. High-temperature gas mixing furnaces were made available by Ed Stolper, and John Beckett kindly introduced me into their operation. I also wish to thank Sieger van der Laan, John Stone, Laurinda Chamberlin, Phil Ihinger, and Mike Wolf for their support and hospitality at Caltech. The manuscript was improved by reviews by George Rossman, Catherine McCammon, Don Dingwell, and B.O. Mysen. This is Caltech Division of Geological and Planetary Sciences contribution number 4899.

References cited

Ahmed, A.A., Abbas, A.F., and Moustafa, F.A. (1983) The mixed alkali effect as exhibited in the spectra of borate glasses containing Cu^{2+}. Physics and Chemistry of Glasses, 24, 43–46.

Alyea, E.C., Basi, J.S., Bradley, D.C., and Chisholm, M.H. (1971) Covalent compounds of quadrivalent transition metals. Part II. Chromium(IV) tertiary alkoxides and triethylsilyloxide. Journal of the Chemical Society, A, 1971, 772–776.

Bansal, N.P., and Doremus, R.H. (1986) Handbook of glass properties, 680 p. Academic Press, New York.

Barnes, S.J. (1986) The distribution of chromium among orthopyroxene, spinel, and silicate liquid at atmospheric pressure. Geochimica et Cosmochimica Acta, 50, 1889–1909.

Boon, J.A., and Fyfe, W.S. (1972) The coordination number of ferrous ions in silicate glasses. Chemical Geology, 10, 287–298.

Burns, R.G. (1970) Mineralogical applications of crystal field theory, 224 p. Cambridge University Press, Cambridge, United Kingdom.

——— (1985) Thermodynamic data from crystal field spectra. In Mineralogical Society of America Reviews in Mineralogy, 14, 277–316.

Burns, R.G., and Fyfe, W.S. (1964) Site of preference energy and selective uptake of transition-metal ions from a magma. Science, 144, 1001–1003.

Calas, G., and Petiau, J. (1983) Structure of oxide glasses: Spectroscopic studies of local order and crystallochemistry. Geochemical implications. Bulletin de Minéralogie, 106, 33–55.

Ciampolini, M. (1966) A crystal field model for high-spin five-coordinated nickel(II) complexes. Inorganic Chemistry, 5, 35–40.

Colson, R.O., McKay, G.A., and Taylor, L.A. (1988) Temperature and composition dependencies of trace element partitioning: Olivine/melt and low-Ca pyroxene/melt. Geochimica et Cosmochimica Acta, 52, 539–553.

——— (1989) Charge balancing of trivalent trace elements in olivine and low-Ca pyroxene: A test using experimental partitioning data. Geochimica et Cosmochimica Acta, 53, 643–648.

Cooney, T.F., and Sharma, S.K. (1990) Structure of glasses in the systems Mg_2SiO_4-Fe_2SiO_4, Mn_2SiO_4-Fe_2SiO_4, Mg_2SiO_4-$CaMgSiO_4$, and Mn_2SiO_4-$CaMnSiO_4$. Journal of Non-Crystalline Solids, 122, 10–32.

Corrias, A., Magini, M., de Moraes, M., Sedda, A.F., Musinu, A., Paschina, G., and Piccaluga, G. (1986) X-ray diffraction investigation of Co(II) ions in borosilicate glasses. Journal of Chemical Physics, 84, 5769–5774.

Dingwell, D.B., and Webb, S. (1990) Relaxation in silicate melts. European Journal of Mineralogy, 2, 427–449.

Durán, A., and Fernández Navarro, J.M. (1985) The colouring of glass by Cu^{2+} ions. Physics and Chemistry of Glasses, 26, 126–131.

Dyar, M.D., and Birnie, D.P. (1984) Quench media effects on iron partitioning and ordering in lunar glass. Journal of Non-Crystalline Solids, 67, 397–412.

Dyar, M.D., Naney, M.T., and Swanson, S.E. (1987) Effects of quench methods on Fe^{2+}/Fe^{3+} ratios: A Mössbauer and wet-chemical study. American Mineralogist, 72, 792–800.

Figgis, F.N. (1966) Introduction to ligand fields, 351 p. Interscience, New York.

Fox, K.E., Furukawa, T., and White, W.B. (1982) Transition metal ions in silicate melts. Part 2. Iron in sodium silicate glasses. Physics and Chemistry of Glasses, 23, 169–178.

Furlani, C. (1968) Ligand field interpretation of some cases of pentacoordination. Coordination Chemistry Reviews, 3, 141–167.

Galoisy, L., and Calas, G. (1991) Nickel speciation in quenched silicate melts. Fourth Silicate Melt Workshop Program and Abstracts, March 19–23, 1991, Le Hohwald, Alsace, France.

Goldman, D.S., and Berg, J.I. (1980) Spectral study of ferrous iron in Ca-Al-borosilicate glass at room and melt temperatures. Journal of Non-Crystalline Solids, 38/39, 183–188.

Goldman, D.S., and Rossman, G.R. (1977) The spectra of iron in orthopyroxene revisited: The splitting of the ground state. American Mineralogist, 62, 151–157.

Hart, S.R., and Davis, K.E. (1978) Nickel partitioning between olivine and silicate melt. Earth and Planetary Science Letters, 40, 203–219.

Henderson, P., and Dale, I.M. (1970) The partitioning of selected transition element ions between olivine and groundmass of oceanic basalts. Chemical Geology, 5, 267–274.

Hu, X., Langer, K., and Boström, D. (1990) Polarized electronic absorption spectra and Ni-Mg partitioning in olivines $(Mg_{1-x}Ni_x)_2SiO_4$. European Journal of Mineralogy, 2, 29–41.

Irving, A.J. (1978) A review of experimental studies of crystal/liquid trace element partitioning. Geochimica et Cosmochimica Acta, 42, 743–770.

Kinzler, R.J., Grove, T.L., and Recca, S.I. (1990) An experimental study on the effect of temperature and melt composition on the partitioning of nickel between olivine and silicate melt. Geochimica et Cosmochimica Acta, 54, 1255–1265.

Kohn, S.C., Charnock, J.M., Henderson, C.M.B., and Greaves, G.N. (1990) The structural environments of trace elements in dry and hydrous silicate glasses: A manganese and strontium K-edge X-ray absorption spectroscopic study. Contributions to Mineralogy and Petrology, 105, 359–368.

Kojima, K., Matsuda, J., and Kimura, T. (1988) Electronic spectral study of Co(II) complexes in potassium borate glasses with low alkali oxide contents. Physics and Chemistry of Glasses, 29, 154–156.

König, E. (1971) The nephelauxetic effect. Calculation and accuracy of the interelectronic repulsion parameters I. Cubic high-spin d^2, d^3, d^7, and d^8 systems. Structure and Bonding, 9, 175–212.

Lin, T.C., and Angell, A. (1984) Electronic spectra and coordination of Ni^{2+} in potassium borate glass and melt to 1000 °C. Communications of the American Ceramic Society, 67, 33–34.

Mao, H.K., and Bell, P.M. (1975) Crystal-field effects in spinel: Oxidation states of iron and chromium. Geochimica et Cosmochimica Acta, 39, 865–874.

Morassi, R., Bertini, I., and Sacconi, L. (1973) Five-coordination in iron(II), cobalt(II), and nickel(II) complexes. Coordination Chemistry Reviews, 11, 343–402.

Mysen, B.O., and Virgo, D. (1989) Redox equilibria, structure, and properties of Fe-bearing aluminosilicate melts: Relationships among temperature, composition, and oxygen fugacity in the system Na_2O-Al_2O_3-SiO_2-Fe-O. American Mineralogist, 74, 58–76.

Nelson, C., and White, W.B. (1980) Transition metal ions in silicate melts. I. Manganese in sodium silicate melts. Geochimica et Cosmochimica Acta, 44, 887–893.

——— (1986) Transition metal ions in silicate melts. IV. Cobalt in sodium silicate and related glasses. Journal of Materials Research, 1, 130–138.

Nelson, C., Furukawa, T., and White, W.B. (1983) Transition metal ions in glasses: Network modifiers or quasi-molecular complexes? Materials Research Bulletin, 18, 959–966.

Oyamada, R., Kishioka, A., and Sumi, K. (1987) Optical absorption spectra of Ni^{2+} and IR spectra in $(100 - x)(PbO \cdot GeO_2) \cdot xR_2O$ (R = Mg, Ca, Sr, Ba) glasses. Journal of Non-Crystalline Solids, 95/96, 709–716.

Rao, B.G., and Rao, K.J. (1986) The study of oxidation state of manganese in lead oxyhalide glasses by optical spectroscopy. Journal of Materials Science Letters, 5, 141–143.

Rossman, G.R. (1988) Optical spectroscopy. In Mineralogical Society of America Reviews in Mineralogy, 18, 207–254.

Rossman, G.R., Shannon, R.D., and Waring, R.K. (1981) Origin of the yellow color of complex nickel oxides. Journal of Solid State Chemistry, 39, 277–287.

Scheetz, B.E., and White, W.B. (1972) Synthesis and optical absorption spectra of Cr^{2+}-containing orthosilicates. Contributions to Mineralogy and Petrology, 37, 221–227.

Schmetzer, K. (1982) Absorptiosspekroskopie und Farbe von V^{3+}-haltigen natürlichen Oxiden und Silikaten—ein Beitrag zur Kristallchemie des Vanadiums. Neues Jahrbuch für Mineralogie Abhandlungen, 144, 73–106.

Schreiber, H.D. (1977) On the nature of synthetic blue diopside crystals: The stabilization of tetravalent chromium. American Mineralogist, 62, 522–527.

Schreiber, H.D., and Haskin, L.A. (1976) Chromium in basalts: Experimental determination of redox states and partitioning among synthetic silicate phases. Proceedings of the Seventh Lunar Science Conference, 1221–1259.

Schreiber, H.D., Thanyasiri, T., Lach, J.J., and Legere, R.A. (1978) Redox equilibria of Ti, Cr, and Eu in silicate melts: Reduction potentials and mutual interactions. Physics and Chemistry of Glasses, 19, 126–139.

Seth, V.P., and Yadav, A. (1987) Electron spin resonance and optical spectra of VO^{2+} and Cu^{2+} in $SrO\text{-}B_2O_3$ glasses. Physics and Chemistry of Glasses, 28, 109–111.

Shannon, R.D. (1976) Revised effective ionic radii and systematic studies of interatomic distances in halides and chalcogenides. Acta Crystallographica, A32, 751–767.

Spiering, B., and Seifert, F.A. (1985) Iron in silicate glasses of granitic composition: A Mössbauer spectroscopic study. Contributions to Mineralogy and Petrology, 90, 63–73.

Takahashi, E. (1978) Partitioning of Ni^{2+}, Co^{2+}, Fe^{2+}, Mn^{2+}, and Mg^{2+} between olivine and silicate melts: Compositional dependence of partition coefficients. Geochimica et Cosmochimica Acta, 42, 1829–1845.

Turner, W.H., and Turner, J.A. (1972) Ligand-field spectra and structure of nickel in silicate glasses. Journal of the American Ceramic Society, 55, 201–207.

Watson, B.E. (1976) Two-liquid partition coefficients: Experimental data and geochemical applications. Contributions to Mineralogy and Petrology, 56, 119–134.

Waychunas, G.A., Brown, G.E., and Apted, M.J. (1986) X-ray K-edge absorption spectra of Fe minerals and model compounds: II. EXAFS. Physics and Chemistry of Minerals, 13, 31–47.

Waychunas, G.A., Brown, G.E., Ponader, C.W., and Jackson, W.E. (1988) Evidence from X-ray absorption for network-forming Fe^{2+} in molten alkali silicates. Nature, 332, 251–253.

White, W.B., and Knight, D.S. (1986) Transition metal ion species in glass: A comparison of optical absorption and luminescence evidence. Proceedings of the Materials Research Society, 61, 283–293.

Wong, J., and Angell, C.A. (1976) Glass structure by spectroscopy, 864 p. Dekker, New York.

Wood, J.S. (1972) Stereochemical and electronic structural aspects of five-coordination. Progress in Inorganic Chemistry, 16, 227–486.

Manuscript received August 8, 1990
Manuscript accepted September 9, 1991